Tip-sample interaction effects in scanning-tunneling and atomic-force microscopy

S. Ciraci* and A. Baratoff
IBM Research Division, Zurich Research Laboratory, Säumerstrasse 4, CH-8803 Rüschlikon, Switzerland

Inder P. Batra
IBM Research Division, Almaden Research Center, 650 Harry Road, San Jose, California 95120-6099
(Received 20 July 1989)

We present a theoretical analysis of tip-sample interactions in scanning-tunneling and atomic-force microscopy with atomic resolution, based on *ab initio* calculations of electronic structure, total energy, and forces. Our results for model systems consisting of a graphite monolayer and of 2×2 or 3×3 arrays of aluminum-tip atoms at high-symmetry sites indicate that at separations below 4 Å the tip already induces changes in electronic structure accompanied by significant charge rearrangements. In particular, site-specific localized states appear and provide a net binding interaction. Because the tip admixes states different than those near the Fermi level of pristine graphite, the tunneling current can deviate considerably from the commonly assumed proportionality to the local density of states of the unperturbed sample. Drastic changes occur at shorter distances where an overall repulsion prevails and where most measurements have been made to date. The ion-ion repulsion is found to determine the force corrugation in that range and up to the separation corresponding to maximum attraction. For the system considered here, the net attractive force on the tip and the corresponding gradient are weaker at the top site than at the hollow site.

I. INTRODUCTION

The invention of scanning-tunneling microscopy[1] (STM) and subsequently of atomic-force microscopy[2] (AFM) opened up new horizons in studying the structure and the electronic properties of both well-ordered and partially disordered solid surfaces down to the atomic scale. Early theoretical studies focused on the resolution obtainable with STM, including material- and voltage-dependent effects.[3-6] As documented in a number of conference proceedings,[7-10] the explosive development of experimental studies and applications based on those techniques has been accompanied by comparatively few theoretical studies, however. In earlier studies, the focus of attention was the resolution obtainable with STM. Starting from Bardeen's transfer Hamiltonian formalism[11] and representing the tip by a single s wave, Tersoff and Hamann[3] showed that the tunneling current and thus STM images are approximately related to the local density of the electronic states of the sample at the center of the tip, $\rho_s(\mathbf{r}_0,E_F)$. This quantity may differ from the total surface charge density, $\rho_s(\mathbf{r}_0)$, especially in the case of semiconductors and semimetals.[4,5,12] In fact, dramatic evidence for the importance of this difference has emerged from STM studies of the cleaved graphite surface.[5,13-15] The crucial effect of the shape of the tip of STM images of graphite has been explained in similar terms by Mizes *et al.*[16] Furthermore, the large current-dependent corrugation obtained from an STM study[17] of graphite indicated the importance of tip-sample forces causing different local elastic deformations of the sample.

The first-order perturbation approach used in the above theories[3-6,12,15] assumes sufficiently spaced, nearly independent electrodes. However, the observation of force variations of order 10^{-9} N, i.e., several eV/Å, while the tip is scanned under typical STM operating conditions[18] implies significant overlap and even rearrangements between the electronic charge densities of sample and tip, at least if just a few atoms are responsible for these variations. Since the latter are similar to those typically involved in AFM experiments,[18,19] the same issue arises in that context. At small *tip-sample separation* h (i.e., at small bias voltage V or current I) a simple relation between STM images and the electronic structure of the unperturbed sample, i.e., $\rho_s(\mathbf{r}_0,E_F)$, is therefore questionable. Earlier self-consistent-field (SCF) pseudopotential calculations[20] have shown that as h is decreased, the potential barrier Φ gradually collapses, and the surface charge density of graphite is locally disturbed. This even leads to a chemical bond (or contact) between a carbon atom simulating the outermost atom on the probing tip and the nearest surface atom if h is close to a nearest-neighbor C-C distance. At the same time Tekman and Ciraci[21] studied effects of tip-sample interactions in the same system within the empirical tight-binding approximation, and provided additional insight into the formation and evolution of *tip-induced localized states* (TILS) as a function of h at high-symmetry sites. They were able to distinguish three regimes depending on the value of h (namely, contact or chemical bond, TILS, and nearly independent electrodes), and showed that STM contrast can be significantly enhanced in the presence of TILS. This was demonstrated in calculations based on a generalization of the Tersoff-Hamann approach[3] which properly includes contributions from TILS concentrated near the tip or the sample.[21] An instructive way to look at the latter is to think of the tip as creating a local perturbation in the potential near the surface of the sample. Just like a

surface defect,[22] this perturbation can lead to localized states or resonances with enhanced amplitude in the vicinity of the tip and to an anomalous h dependence of STM images. One important difference is that the perturbation is dragged along as the tip is scanned over the sample. The observed modulation in h (at constant tunnel current I), or in I itself (at constant mean current) therefore reflects in part *changes* in *electronic structure* due to the varying local environment of the tip.

The influence of tip-surface interactions on electronic structure is initiated by the lowering of the intervening potential barrier, which is appreciable (but not easily detectable)[23] already at separations h larger than in the typical STM operating range. The gradual collapse of the barrier as h is decreased and its delayed effect on the tunnel current have been illustrated nicely by studies of the transition from tunneling to essentially single-atom contact between metallic tip and sample[24] and by calculations of adatoms on jellium substrates.[25] More recently, increasingly stronger attraction up to the adhesion minimum was shown to occur over essentially the same h range in a combined STM-AFM experimental study.[26] Finally, STM observations of individual "atoms" with the expected periodicity on nominally flat (111) surfaces of close-packed noble and simple fcc metals[27,28] with a corrugation much larger than one would deduce from $\rho_s(\mathbf{r}_0)$ suggest site-dependent electronic tip-surface interaction effects. Whether force variations and induced deformations along STM scans[17] and/or changes in electronic structure[29] must be invoked to explain such observations is understandably a matter of increasing concern.

The interpretation of the corrugation measured in AFM has also been controversial, especially in the case of graphite.[19] Atomic resolution has so far been achieved with repulsive forces of 10^{-6}–10^{-8} N. Such strong forces appear sufficient to cause the plastic deformations, unless they are distributed over many surface atoms.[30] This may occur if the tip slides over a thin contamination layer,[31] or if it drags along a foreign particle or a flake of several deformed graphite layers.[30] Even if only the outermost tip atom is acting, it is commonly assumed that force variations are primarily determined by the repulsive interaction which is, in turn, approximately proportional to the electronic charge density of the free surface $\rho_s(\mathbf{r}_0)$. Recent theoretical studies have been at variance with this simple picture. Apart from distortions due to the tip shape,[32,33] atomic-force calculations[20] indicated that beyond a certain separation the magnitude of the force on the tip at the hollow site of graphite can exceed that at the atomic sites.

In this study we present a thorough analysis of tip-sample interaction effects based on *ab initio* SCF-pseudopotential calculations like those initiated earlier.[20] In view of computational limitations such calculations are performed with periodically repeated supercells containing 9–22 atoms. In Ref. 20 results were reported for a (1×1) array of carbon atoms, each one representing the outermost atom of the tip, at two high-symmetry positions with respect to three layers of graphite. Since the main features of the electronic structure of graphite are determined by that of a single monolayer and since the tip was found to exert forces on top-layer atoms only, we have performed calculations of electronic charge densities, total energy, and atomic forces for a graphite monolayer and larger arrays of single-atom and multiatom aluminum tips. Similar calculations for a (2×2) array of carbon atoms and of graphite lattice deformations induced by localized forces[34] will be reported elsewhere.

The (0001) surface of graphite is an interesting sample for a number of reasons, already discussed in the context of STM (Refs. 5, 12–17, and 20–22) and AFM.[18–20,33,34] From a theoretical viewpoint, its structure leads to dramatic electronic[12,20,21] and lattice deformation[17,33,34] effects which are also expected in other layered materials. From an experimental point of view, broad flat areas of this rather inert surface are easily exposed by cleavage. This permits rapid recording of tunneling current and force (or force gradient) variations at *constant mean* values of these quantities, i.e., approximately constant mean tip-sample separation,[35] as well as conventional "topographic" images at constant local values of these quantities. Although many investigations have achieved "atomic resolution" in air and even in (presumably) inert liquids,[36] their interpretation has been confused by the role played by poorly specified contamination layers[31] or particles.[30] To resolve these as well as more fundamental issues, it seems appropriate to return to studies under better controlled conditions. Most theoretical results, including the present ones, can only be meaningfully compared to measurements with well-characterized tips in UHV. Unfortunately only a few STM studies of graphite in UHV have been performed to date.[13,14] Aluminum is chosen for our tip mainly because it is a simple metal without d states which are easily handled within a pseudopotential scheme. It is also sufficiently hard for use as tip material in actual STM or AFM experiments. Finally we also wanted to understand tip-sample interaction effects between different materials, as well as the influence of metallic bonding of the outermost atom to the rest of the tip.

Our purpose is twofold: first, to provide a more realistic description and a deeper understanding of interatomic forces on the tip and nearby atoms of the sample; second, to give a more systematic account of changes in the potential energy, charge density, and electronic structure as a function of tip position in a self-consistent framework. Consequences of the first and second aspects for STM and AFM are discussed with an eye towards deviations from commonly accepted notions. Lattice deformations and related effects are not considered here. As might be expected, at sufficiently small tip-sample separations h, the force on the outermost tip atom is dominated by the ion-ion repulsion. The latter is stronger at the top site than at the hollow site and exceeds the attractive force due to the interaction of the tip with the electronic density of the sample (including changes induced by the tip). In the end one obtains a larger net repulsive force and, further away, a weaker attractive force at the top site as compared to the hollow site. The same behavior is predicted for the force gradient, except that its maximum occurs at larger h. Accordingly a tip scanning in the *constant-distance* mode of AFM images surface atoms as

repulsive maxima or as attractive minima. The corrugation at *constant force* is reversed at larger h but this cannot be observed due to an elastic instability of the required soft tip-bearing cantilever.[18,19]

We also examine the formation, energy shifts, and splittings of electronic states as the tip approaches the graphite sample. Our calculations indicate that, 2–4 Å away from the sample, the tip can induce several different site-specific states which become increasingly localized in the vicinity of the tip as h is decreased. Some of them become occupied and form bonds responsible for the minimum in the interaction energy, $\Delta E(h)$. The effect of the tip can be so dramatic that the tunneling conductance at small voltage, which is determined by states at the corners of the Brillouin zone (BZ) if tip-sample interactions are neglected,[5,12–16] becomes dominated by the admixture of different states within a few eV of the Fermi level. In this fashion a significant tunneling current can arise even if the tip faces the hollow site, where $\rho_s(\mathbf{r}_0,E_F)$ is very low.

II. DESCRIPTION OF THE MODEL

Our results are extracted from *ab initio* calculations for periodically repeated supercells 18 a.u. high along (001), each containing several graphite monolayer cells representing the sample and a tip consisting of one or four Al atoms. The periodic boundary conditions imposed are artificial, but allow us to use a plane-wave basis. In a given layer of graphite there are actually two inequivalent atomic sites, usually denoted as the B and the A sites.[14] The A site has one carbon atom directly below and above it in adjacent layers, whereas the B site does not. The center of the hexagon is usually denoted as the hollow or H site. Since previous calculations[20] showed that tip-surface interaction forces predominantly act on the top graphite layer, the graphite surface is represented by a monolayer. The A and B sites then become equivalent, and are henceforth denoted as the B site. Considering only one layer reduces the number of plane waves required in the z direction perpendicular to the layer, and allows us to use larger lateral supercells in order to better decouple the atoms of the tip array. Most results have been obtained for the graphite $+(2\times2)$ Al model, where each supercell contains one Al atom representing the metal tip positioned above a B, or an H site near the center of 4 graphite monolayer cells, so that the lateral repeat period is 9.3 a.u., i.e., twice as large as in Ref. 20. As a result the range of tip-sample separation h (from 2.74 to 8 a.u.) in which lateral interactions are negligible is also larger. The smallest h (2.74 a.u.), investigated corresponds to the sum of the covalent radii of carbon and aluminum atoms at the H site. Since a smaller h would lead to overlapping of the ionic pseudopotentials, while very large h would require a thick vacuum region where the plane-wave basis becomes inadequate, the range of h must be limited anyway. For purposes of comparison, we also made calculations for $h=3.84$ a.u. with (3×3) supercells consisting of 9 graphite monolayer cells and either one [graphite $+(3\times3)$ Al] or four Al atoms [graphite $+(3\times3$ Al_4] representing the metal tip; the lateral repeat period is then 13.95 a.u. In the case of the multiatom tip, the closest Al atom is at a distance h from the sample and aligned with the center of the triangle formed by the other three Al atoms so as to preserve the local configuration of bulk Al along the [111] axis. The triangle of Al atoms is rotated by $\pi/3$ relative to the triangle formed by the nearest neighbors of the B sites in the graphite monolayer. The same orientation is used at the H site, so that both configurations have the same C_3 rotation symmetry.

Our electronic structure, total energy, and atomic-force calculations were performed using the SCF-pseudopotential approach in momentum space[37] within the local-density approximation (LDA). We used the nonlocal, norm-conserving ionic pseudopotentials proposed by Hamann *et al.*[38] Details of the method and relevant references can be found in Refs. 20, 39, and 40. In the graphite $+(2\times2)$ Al model, plane waves with kinetic energy $|\mathbf{k}+\mathbf{G}|^2\leq9$ Ry were treated exactly, and those with $9<|\mathbf{k}+\mathbf{G}|^2\leq13$ Ry were included via the Löwdin perturbation scheme. This results in a basis set of ~1100 plane waves. Owing to the larger supercell dimensions of the graphite $+(3\times3)$ Al and Al_4 models, Bloch states were expanded in terms of ~1400 plane waves corresponding to a somewhat smaller kinetic energy cutoff, $|\mathbf{k}+\mathbf{G}|^2\leq8.7$ Ry. Since the carbon atom is lacking core states of p symmetry, its ionic pseudopotential is strong, and thus full convergence of absolute total energies would require a much larger plane-wave basis set than used in our calculations.[41] However, binding energies and site-dependent differences obtained from differences of total energies or forces calculated with the same unit cell and cutoff are expected to be reliable when comparing trends. In the self-consistency iterations the charge density was sampled at 64 $\mathbf{k}$ points uniformly distributed in the surface BZ of graphite. In calculating atomic forces we used a more stringent self-consistently criterion (rms deviation in the potential energy $<\sim10^{-7}$ Ry).

III. INTERACTION ENERGY AND ATOMIC FORCES

The graphite surface is rather inert, and thus it is not obvious whether even a single Al atom can be bound on this surface. Our calculations indicate that the binding is weak. The calculation of the interaction energy requires separate computations of the total energies of the graphite monolayer $E_T[\mathrm{C}]$, of the Al tip array $E_T[\mathrm{Al}]$, and that of the combined system for a given tip-sample distance h, $E_T[\mathrm{C+Al};h]$. The minimum of the interaction energy

$$\Delta E(h)=E_T[\mathrm{C+Al};h]-E_T[\mathrm{C}]-E_T[\mathrm{Al}] \quad (1)$$

yields the binding energy E_b. In Fig. 1 calculated values of $\Delta E(h)$ are illustrated for the Al atom facing the B, and the H site in the graphite $+(2\times2)$ Al model. Due to differences in the local atomic arrangement of the substrate detected by the tip, the interaction energy at different sites cannot be merely represented by a universal function shifted along the z axis.[19,26] The binding energies are rather small: $E_b\simeq24$ mRy (0.33 eV) for the B site, and $E_b\simeq45$ mRy (0.61 eV) for the H site. As expect-

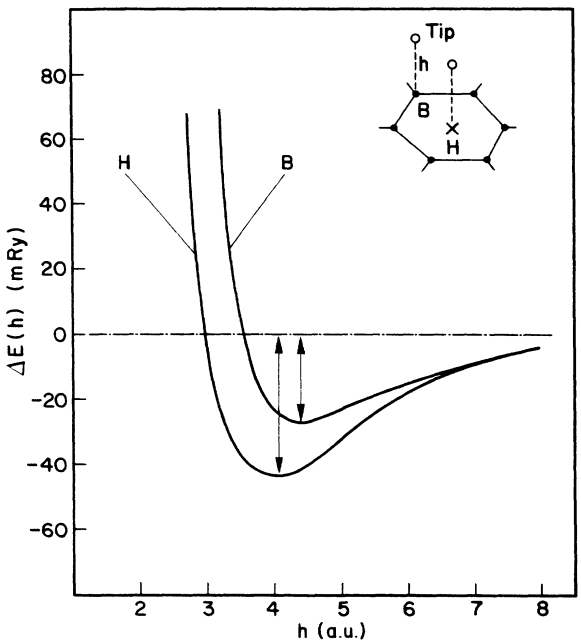

FIG. 1. The interaction energy ΔE per Al atom in a (2×2) array with a graphite monolayer versus separation h at the B and the H sites; arrows indicate the binding energy. The two geometries are shown in the inset.

ed, $\Delta E^H \rightarrow \Delta E^B$ as $h \rightarrow \infty$. The small value of the binding energy E_b at either site is the manifestation of the fact that the graphite surface is inert. Indeed, as will become clear from the discussion in Sec. IV, only a limited number of graphite states can effectively interact with Al states.

Owing to the smaller ion-ion repulsion at the H site (as compared to the B site) and to the relatively large radius of Al orbitals interacting with six (as compared to one plus three) nearby carbon atoms in the graphite monolayer atoms, E_b^H exceeds E_b^B. Furthermore, ΔE^B is much larger than ΔE^H for $h \lesssim 3$ a.u. In the graphite $+(3\times3)$ Al_4 model, $|\Delta E^H - \Delta E^B|$ is found to be 40% smaller than for the graphite $+(2\times2)$ Al model for $h=3.84$ a.u. It appears that metallic binding among the four Al atoms representing the tip redistributes the electronic charge causing the Al-graphite bond to be less localized and the tip-sample interaction to weaken. As a result, the difference between the B and the H sites also becomes less pronounced. A similar effect accompanying the metallization of the overlayer was pointed out earlier for the Al-Ge(100) interface.[42] At large tip-sample distances ($h \gtrsim 8$ a.u.) the present approach cannot yield an accurate value for ΔE. First, lateral interaction between artificially repeated Al tip atoms exceed tip-sample interactions and weaken the latter. Second, in the resulting thick vacuum region between the surface and the Al atoms the tails and residual overlap of wave functions are poorly represented. Finally, because the total charge density becomes very low ($\rho \simeq 10^{-5}$–10^{-6} a.u.), the local-density approximation to the exchange and correlation potential becomes inappropriate. Nevertheless, LDA predicts an attractive interaction in the range $\sim 4 < h < 8$ a.u., where it is still expected to be a reasonable approximation. Anyway, for $h \gtrsim 7$ a.u. the two curves $\Delta E^B(h)$ and $\Delta E^H(h)$ essentially merge, leaving a site-independent attraction, as expected if attraction is attributed to long-range polarization forces and repulsion to overlap between neutral atoms. In this range of h the interaction between the sample and an Al atom (or the metal tip) is better represented by the sum of an attractive Van der Waals (or electron correlation) energy, U_{VW}, and of a repulsive energy arising from the orthogonalization of weakly overlapping tip and sample states.[43,44]

According to the Hellman-Feynman theorem,[45] the force on a given atom at position τ_t in the supercell, calculated from $-\partial E_T(\mathrm{C+Al})/\partial\tau_t$ must agree with the expectation value of the gradient of the Hamiltonian, provided that the electronic ground state is accurately calculated, i.e., if self-consistency has been achieved. In the pseudopotential method implemented in momentum space[39,40] within the local-density approximation, the resulting expression for the atomic force has two components. The first one, $\mathbf{F}_{io}$, originates from the Coulomb repulsion between the ion cores, and the second one, $\mathbf{F}_{el}$, is due to the interaction of valence electrons with the ion cores. At small h, $\mathbf{F}_{io}$ is stronger and varies more rapidly than $\mathbf{F}_{el}$ with the position of the outermost tip atom.

Atomic forces on the tip $\mathbf{F}_t$, and on its graphite neighbors within the supercell have been calculated for several tip positions at the B and H sites. Results for the perpendicular components are listed in Table I, and illustrated in Fig. 2 for the graphite $+(2\times2)$ Al model. It is seen that calculated forces on the tip and on the sample balance each other within $\pm 0.2\times10^{-9}$ N. For a given h in the repulsive range, the tip force at the B site F_t^B is larger than that at the H site F_t^H. By contrast, in the attractive range the magnitude of the tip force at the H site is

TABLE I. Binding energy E_b, the tipe force (F_t), and perpendicular components of the forces ($F_{g,1}$) and ($F_{g,2}$) on the first and second neighbors of the tip in the graphite monolayer calculated as a function of h for the graphite $+(2\times2)$ Al model.

H (a.u.)	E_b (m Ry)	F_t (10^{-9} N)	$F_{g,1}$	$F_{g,2}$
		B site		
2.74	418	42.427	−37.769	−1.585
3.20	108	16.899	−15.074	−0.830
3.84	−21	2.904	−3.667	0.041
4.70	−26	−0.350	−0.041	0.159
6.00	−17	−0.473	0.252	0.070
8.00	−4	−0.185	0.049	0.017
		H site		
2.74	122	14.532	−2.552	0.279
3.84	−43	0.762	−0.155	−0.038
4.20	−43	−0.125	0.078	−0.307
4.70	−37	−0.552	0.200	−0.433
6.00	−18	−0.524	0.131	−0.200
8.00	−4	−0.183	0.023	−0.009

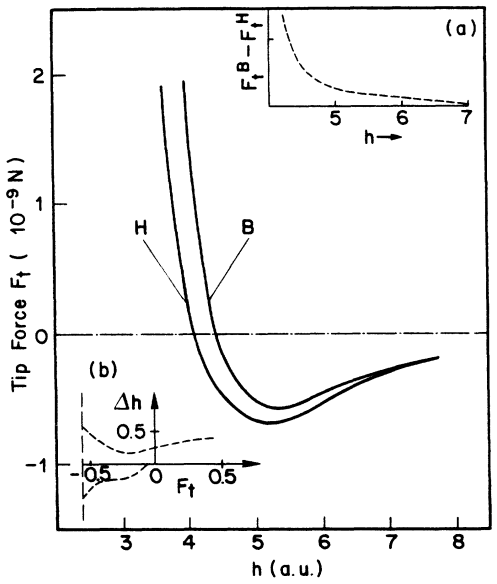

FIG. 2. The z component of force F_t exerted on the tip represented by a single Al atom versus separation at the B and the H sites. Insets (a) and (b) show the difference versus h and the maximum corrugation at constant F_t versus F_t, respectively.

larger. In inset (a) of Fig. 1 we also show $F_t^B - F_t^H$, which is quite large at small h but becomes negligible for $h \gtrsim 7$ a.u. These large differences will tend to be accommodated by deformation if the substrate is allowed to relax. Another interesting consequence is illustrated in inset (b) where $\Delta h = h^B - h^H$ (the difference of tip z displacements for a given force) is plotted. It is readily apparent from the generic form of $F_t(h)$ that $\Delta h(F)$ is a single-valued, slowly increasing, and positive function for $F_t > 0$. This implies that in the constant-force mode the cantilever of an AFM would deflect more at the B site than at the H site. According to this picture the maximum corrugation between B site and H site is ~0.2–0.3 Å (or ~0.4–0.6 a.u.) in agreement with the corrugation of the graphite charge density in the same h range,[5,14,15] as expected if the repulsive interaction is proportional to $\rho_s(\mathbf{r}_0)$. However, in the attractive range, i.e., $F_t < 0$, $\Delta h(F)$ is double valued. While the above-mentioned trend persists on the positive branch except for an increased corrugation near the minimum of F_t, the negative branch is nearly the reverse of the positive branch. Although this idealized description suggests the possibility of observing two opposite corrugations, this will be difficult to observe for the following reasons. First, as we argue at the end of this section, the difference between F_t^B and F_t^H for h beyond maximum attraction becomes less pronounced for an actual tip. Second, a soft cantilever with a soft spring constant k is mechanically unstable[19] in the range where $\partial F_t/\partial h + k < 0$ and jumps towards (away from) the sample as h decreased (increased). With a stiff cantilever, on the other hand, no instability is expected because the effective spring constant of graphite alone exceeds 5 N/m according to several independent calculations[17,33,34] and is thus larger than $\partial F_t/\partial h$ throughout the attractive range. Furthermore, our results indicate that for $h > 7$ a.u. (in the far attractive region), $|F_t^B| > |F_t^H|$. The crossing of the calculated force curves was also obtained in an earlier study[20,34] of the carbon tip, but at a somewhat smaller value of h. From this crossover it follows that at large values of h the tip samples the total charge density of the substrate (exceeding the ion-ion repulsion contribution).

In order to understand the behavior of the force on the tip and to relate it to relevant quantities such as the charge density, we consider the atomic-force expression in real space. According to the Hellmann-Feynman theorem,[45] atomic forces are obtained by differentiating those terms in the Hamiltonian which explicitly depend on the position of the ions. Within the periodic slab model described in Sec. II the total force on the tip (in atomic units) is

$$\mathbf{F}_t = 2 \sum_{n,k}^{E \le E_F} \int \Psi_{n,k}^*(\mathbf{r}) \left[\sum_{l,j \in \text{tip}} \frac{\partial}{\partial \tau_j} \left[\frac{Z_j}{|\mathbf{R}_l + \tau_j - \mathbf{r}|} \right] \right] \Psi_{n,k}(\mathbf{r}) d\mathbf{r} - \sum_{l,s,\ j \in \text{tip}} \frac{\partial}{\partial \tau_j} \left[\frac{Z_j Z_s}{|\mathbf{R}_l + \tau_s - \tau_j|} \right], \tag{2}$$

where $\mathbf{R}_l$ ranges over superlattice vectors, while τ_s and τ_j denote the position vectors of the sample and tip atoms in the supercell, respectively. The integral in the first term is evaluated in the supercell. This term is the electron-ion contribution, earlier denoted as $\mathbf{F}_{\text{el}}$. The second one is the ion-ion repulsion $\mathbf{F}_{\text{io}}$, which is actually calculated with the Ewald procedure. For widely separated tip and sample the electronic charge density $\rho(\mathbf{r})$ can be viewed as the sum of the free-tip and free-sample charge densities. The electronegativity difference between the tip and the sample leads to a transfer of charge $\Delta\rho_\infty$ even at large h. This sets up an electrostatic interaction between the tip and sample. As the tip approaches the sample, $\rho(\mathbf{r})$ also undergoes a local redistribution to minimize the total electronic energy. The ions of the tip and sample themselves are displaced from their initial positions to attain the lowest total energy at the preset h. The positions of the ions define a point on the Born-Oppenheimer surface. Since the tip-sample combined system is subject to an external force, this point must be determined by constrained minimization. The displacements of the tip and sample ions have significant effects on the corrugation in AFM and STM, and are dealt within separate studies.[29,34] We can write the charge density of the electronically deformed system considered here,

$$\rho(\mathbf{r}) = \sum_{n,k}^{E \le E_F} |\Psi_{n,k}(\mathbf{r})|^2 = \rho_s(\mathbf{r}) + \rho_t(\mathbf{r}) + \Delta\rho(\mathbf{r}) \tag{3}$$

in terms of total electron densities of the free sample

$\rho_s(\mathbf{r})$, the free tip $\rho_t(\mathbf{r})$, and the difference charge density $\Delta\rho(\mathbf{r})$ arising from the tip-surface interactions. We may assume that $\Delta\rho_\infty$ is split between $\rho_s(\mathbf{r})$ and $\rho_t(\mathbf{r})$. Such a separation has to conserve charge, of course, and leaves a $\Delta\rho$ predominantly localized between the sample and the tip at the cost of some charge depletion in both electrodes. To simplify our discussion, we neglect the contributions from $\rho_t(\mathbf{r})$ and $\mathbf{F}_{io}$ evaluated among the tip atoms themselves since they cancel each other for a free tip in equilibrium. Omitting the electrostatic interaction mentioned earlier, which depends on the detailed geometry of the tip in an actual experiment, we are left with the short-range force on the tip:

$$\mathbf{F}_t \simeq 2\int [\rho_s(\mathbf{r})+\Delta\rho(\mathbf{r})] \times \left[\sum_{j\in\text{tip}} \frac{\partial}{\partial\tau_j}\left(\frac{Z_j}{|\tau_j-\mathbf{r}|}\right)\right] d\mathbf{r} - \sum_{s,\, j\in\text{tip}} \frac{\partial}{\partial\tau_j}\left(\frac{Z_j Z_s}{|\tau_j-\tau_s|}\right). \quad (4)$$

The distinction between $\mathbf{R}_l$ and τ_s in Eq. (2) has been circumvented by considering the limit of a single tip facing the sample, i.e., an infinitely large supercell. We first consider a single-atom tip by dropping the j sum in Eq. (4) and discuss the perpendicular component of the resulting force F_t. At small h, $F_{io} > |F_{el}|$ yields a repulsive force. However, as h increases, $|F_{el}|$ decays more slowly than F_{io} and $F_t = F_{el} + F_{io}$ changes sign where $\Delta E(h)$ attains its minimum value, leading to a net attraction. This is mainly caused by the bonding charge density $\Delta\rho$ accumulated between the tip and the sample. In the strong repulsive regime at small h, F_{io} considerably exceeds $|F_{el}|$ at the top site [in spite of the fact that a significant $\Delta\rho(\mathbf{r})$ is present] and is also larger than F_{io} at the hollow site. Consequently, $F_t^B > F_t^H$, and the tip mainly feels the ionic repulsion and therefore images atomic sites as maxima in AFM. In the intermediate range of h, $\Delta\rho(\mathbf{r})$ plays an important role in determining force variations. Therefore, a detailed account of both electronic and ionic contributions is required. Nevertheless, as demonstrated in Fig. 3, $F_{io}^B - F_{io}^H$ is still large enough to compensate the appreciable difference arising from $F_{el}^B - F_{el}^H$ and to yield less attraction on the top site. In this range the tip therefore feels a more attractive force at the hollow site than at the top site. The difference between the ion-ion forces at the B and H sites is greater than that of the electron-ion forces up to $h \simeq 7$ a.u. Beyond this value of h, $F_{io}^B \to F_{io}^H$, and thus $F_{el}^B - F_{el}^H$, appears to win over, but this effect is marginal. The resulting crossing of the force curves is material dependent and affected by lateral interactions, and thus cannot be easily explained or generalized to other tip-sample systems. Moreover, one must be cautious when drawing any qualitative conclusions from our calculations in this region since LDA and our basis set become less reliable at large values of h.

Another important question is whether the shape of the tip (e.g., whether it has one or more outermost atoms) affects the AFM images. As recent model calculations have shown[32] if the tip has two equivalent outermost

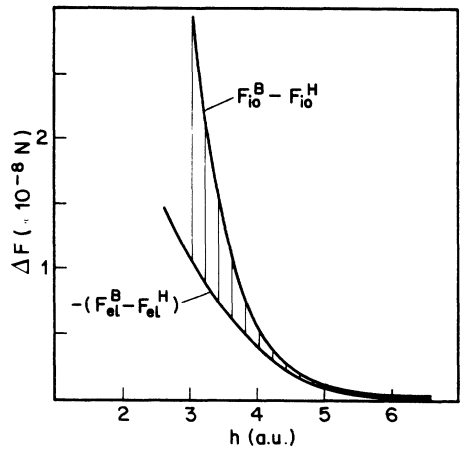

FIG. 3. The variation of the differences between ionic forces F_{io}, and between electronic forces, F_{el}, at the B and the H sites versus h. The shaded area corresponds to $|F_t^B - F_t^H|$ in the inset (a) of Fig. 2.

atoms, the net force on the tip can be well approximated by superposition in a wide range of h. The relative orientation of the tip with respect to the substrate plays an important role, and the detailed structure of the images can be quite different from those obtained with a single atom tip. These calculations[32] indicate, however, that the lateral periodicity (i.e., the unit cell) of the sample surface is always imaged no matter what the orientation of the tip is. The distortions within the unit cell can become quite complicated if h is so small that $\Delta\rho(\mathbf{r})$ changes appreciably. In the case where the tip has a large flat area, the corresponding atoms can be at various lateral positions with respect to the sample unit cell. This tends to smear out the lateral resolution in AFM. As shown by recent molecular-statics calculations,[33] such a flat tip is nevertheless able to image the periodicity of the sample if it consists of the same material or supports a flake thereof.

We finally consider the applicability of calculations such as ours, where the tip is represented by a single atom. Owing to the metallic bond between the outermost atom with the surrounding atoms in a real tip, the net tip-sample force and its corrugation might be significantly altered. In this context, we note that in earlier studies[20] where the tip was represented by a single carbon atom, and the repulsive force F_t was calculated at a separation $h = 2.7$ a.u. corresponding to the nearest-neighbor spacing in graphite, turned out to be 2 orders of magnitude smaller than the loading force in typical AFM measurements.[19] On the other hand, recent molecular-statics[33] and lattice statics studies[34] indicate that the tip forces as low as 10^{-8} N is enough to puncture the top graphite layer. The source of this discrepancy between theory and experiment is to a large part probably due to contact of several tip atoms with an intermediate layer or with the sample surface and, to some extent, to the effect of attractive forces exerted by tip atoms further away than the outermost one, owing to their longer range. The difference between the force on the outermost tip atom

TABLE II. Perpendicular components of forces on the tip atom (F_t), first and second graphite neighbors of the tip ($F_{g,1}$,$F_{g,2}$) calculated at $h=3.84$ a.u. for the graphite $+(3\times3)$ Al model.

	$F_t(10^{-9}$ N)	$F_{g,1}$	$F_{g,2}$
B	4.231	−4.306	−0.049
H	1.802	−0.373	0.051

and the total tip force may change depending on h, the radius of the tip base, and the angle of the tip cone.[26] For example, whenever the outermost tip atom feels a repulsion at small h, attraction by the rest of the tip atoms can force the tip to move even closer. Furthermore the additional attraction can cause the tip to jump towards the sample from a much larger h. Within the LDA this attraction results from the j summation in Eq. (4) over all tip atoms. Forces on atoms further away can be approximated by an integral over body forces. This gives a relatively strong but essentially uncorrugated attraction. A clean extended tip with a protruding atom cannot exert a force in the range of $\sim10^{-7}$ N without plastically deforming the surface.[30] A flat tip may support a large repulsive force, but it is unlikely to lead to atomic resolution.[33] These arguments are justified by the recent measurements of Dürig *et al.*,[26] who estimated tip forces in the range of 10^{-9} N just before contact.

We explored the effect of the multiatom tip by comparing the forces calculated for the graphite $+(3\times3)$ Al and the graphite $+(3\times3)$ Al_4 models, at a distance 3.84 a.u. from the graphite monolayer. While the first one has only a single atom representing the tip as in our graphite $+(2\times2)$ Al model, the second one has four tip atoms with a single outermost atom. Calculated forces on tip atoms and forces on the first- and second-neighbor atoms of graphite relative to the tip are presented in Tables II and III. The force on the outermost atom of the four-atom tip is seen to be larger than that for the single atom tip, for the *B* as well as the *H* site. This is due to the internal forces in the four-atom Al cluster. As a matter of fact, a separate calculation[29] shows that in a free Al_4 pyramid the outermost tip atom is closer to the base than the bulk spacing used in the present calculation. Therefore, the internal force which attracts the apex atom towards the base is added up to give larger repulsion. The most striking difference is found at the H site, where the first atom of the multiatom tip feels a much stronger repulsion compared to the single-atom tip. Just like for the difference between the interaction energies, the force corrugation becomes less pronounced in going from a single to a multiatom tip. This situation is attributed to the greater delocalization of the tip-sample bond upon metallization of the four-atom tip, and to the increased screening of the tip ions. Upon summing the individual forces over the tip atoms, the internal forces cancel out. As a result the total force at the *B* site is smaller than for the single-atom tip due to partial compensation between attraction and repulsion. Moreover the total tip forces are much closer to that on the single-atom tip, but again the difference between the *B* and the *H* sites is less pronounced.

IV. TIP-INDUCED CHANGES IN ELECTRONIC STRUCTURE

In the independent electrode limit corresponding to large h, the assumption that the tip as well as the sample states are unperturbed is justifiable. However, as the tip approaches the sample surface, the overlap of the tip and sample wave functions increases, and a significant interaction sets in. Contours of constant SCF potential $V(x,y,z)$ (i.e., $l=0$ component of pseudopotential plus Hartree plus local exchange-correlation potentials) of the graphite $+(2\times2)$ Al system on a plane parallel to the sample surface and bisecting the tip-to-surface distance are shown in Figs. 4(b) and 4(c) for two values of h. The corresponding contours for bare graphite at the same distance z are shown for comparison to the first case in Fig. 4(a). It is seen that for the tip close to the surface, the potential barrier is significantly lowered and even a channel with $V(x,y,z)<E_F$ connecting the tip to the sample is formed. This can certainly have important implications for the electronic structure as far as STM and AFM are concerned. In what follows we examine other manifestations of the tip-surface interaction.

To understand such effects let us first consider unperturbed sample and tip wave functions φ_s and φ_t with energies $\varepsilon_s=\langle\varphi_s|\mathcal{H}_s|\varphi_s\rangle$ and $\varepsilon_t=\langle\varphi_t|\mathcal{H}_t|\varphi_t\rangle$, respectively. To simplify the picture we also assume that $\langle\varphi_s|\varphi_t\rangle=0$. For the interacting tip-sample system the total Hamiltonian $\mathcal{H}$ differs from the sum of $\mathcal{H}_s$ and $\mathcal{H}_t$. Then, in first-order perturbation theory the interaction energy at a given h is

$$U(h)=-\langle\varphi_s|\mathcal{H}|\varphi_t\rangle\ . \tag{5}$$

When U is small the energies of the independent electrode states shift slightly without a significant mixing. In general the smaller h and $|\varepsilon_t-\varepsilon_s|$, the larger is U. If no other states are significant, the interacting states become bonding and antibonding combinations of the unperturbed tip and sample wave functions, $\Psi=c_s\varphi_s+c_t\varphi_t$.

TABLE III. Perpendicular components of forces on the outermost tip atom ($F_{t,1}$), second layer tip atoms ($F_{t,2}$), first and second graphite neighbors of the tip ($F_{g,1}$,$F_{g,2}$) calculated at $h=3.84$ a.u. for the graphite $+(3\times3)$ Al_4 model.

	$F_{t,1}(10^{-9}$ N)	$F_{t,2}$	$\sum F_{t,i}$	$F_{g,1}$	$F_{g,2}$
B	5.842	−0.830	3.350	−3.113	0.033
H	3.943	−0.725	1.764	−0.348	−0.004

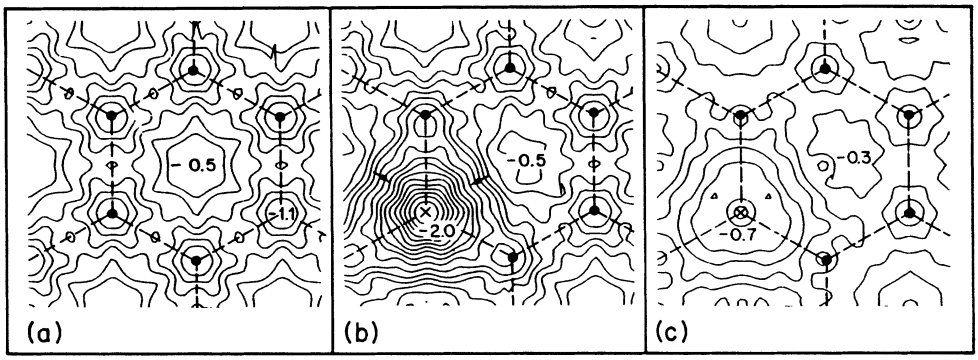

FIG. 4. Contours of constant electron potential energy, $V(x,y,z=h/2)$ ($l=0$ component of the ionic pseudopotential plus Hartree plus local exchange-correlation potential) for (a) the free graphite (0001) surface in a parallel plane 1.92 a.u. above the surface, (b) an Al atom facing the B site at $h=3.84$ a.u. in the same contour plane, (c) the same situation as in (b), but with $h=6$ a.u. in the plane bisecting h. The lateral positions of Al and C atoms are indicated by a cross and by closed circles, respectively. The contour spacing is -0.08 Ry in (a) and (b), and -0.07 Ry in (c), the corresponding Fermi energy being $E_F \simeq -0.22$ Ry. Small arrows show the direction in which the potential becomes more negative.

Defining $\zeta=[4U^2+(\varepsilon_t-\varepsilon_s)^2]^{1/2}$, the perturbation energy is minimized for the coefficients $c_s=c_+$, $c_t=c_-$ and $c_s=c_-$, $c_t=-c_+$, where

$$c_+=[\tfrac{1}{2}+(\varepsilon_t-\varepsilon_s)/2\zeta]^{1/2}\,,$$
$$c_-=[\tfrac{1}{2}-(\varepsilon_t-\varepsilon_s)/2\zeta]^{1/2}\,, \tag{6}$$

where $\varepsilon_\pm=\langle\Psi_\pm|\mathcal{H}|\Psi_\pm\rangle=(\varepsilon_t+\varepsilon_s)/2\mp\zeta/2$. Thus the admixture $1-c_+^2$ is a measure of the deviation from the independent electrode approximation. If $\varepsilon_t\neq\varepsilon_s$, mixing due to $U\neq 0$ results in a transfer of charge. Based on empirical tight-binding calculations of (3×3) arrays of carbon atoms at a distance h above a graphite monolayer, Tekman and Ciraci[21] pointed out that, owing to the local character of the perturbation, Ψ becomes increasingly localized parallel to the surface as h is decreased. For a given parallel wave vector $\mathbf{k}_\parallel$ the states of our model systems are strongly discretized in energy, so that the above discussion can be applied. In the case of a macroscopic sample and of an isolated tip, it continues to make sense if the states in question are derived from states of the topmost graphite layer and from atomiclike resonances of the outermost tip atom.

We now analyze the influence of the tip on the electronic structure of our system in terms of the above discussion. We wish to address the following questions: (i) In what range of h does the tip-surface interaction become significant? (ii) In which positions can the tip preferentially induce TILS in the graphite-Al system? (iii) What might be the consequences of these effects in STM and AFM? We first consider charge densities, and look for interaction effects in the difference charge density. To this end we show calculated contours of difference and total charge densities for the graphite $+(2\times2)$ Al model in a plane containing the Al tip atom and nearest neighbors in the graphite sample in Figs. 5(a) and 5(c) and in a parallel plane bisecting h in Fig. 5(b). The contour plots of $\Delta\rho(\mathbf{r})$ in Fig. 5(a) clearly indicate that at small h the sample and the tip cannot be considered independent. Charge is accumulated between the tip and the nearest surface atom via the bonding states Ψ_+, discussed above.

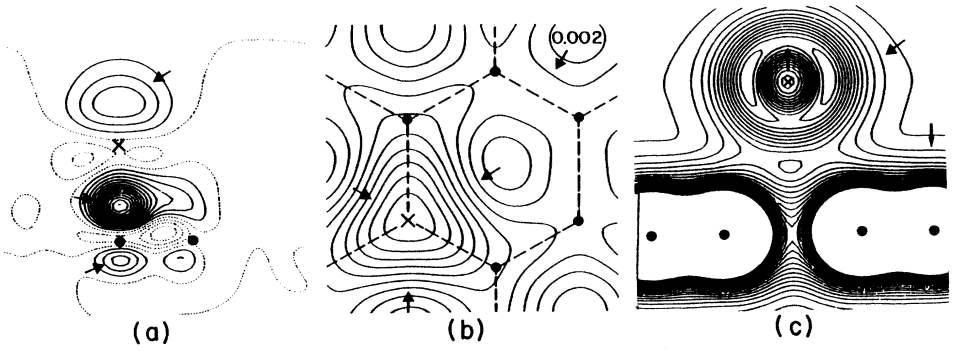

FIG. 5. Contours of constant charge density. (a) Difference of total charge densities—C(2×2)+Al at $h=3.8$ a.u. above the B site minus separated electrodes—in a vertical plane passing through Al and a C—C bond. (b) Total charge density for graphite $+(2\times2)$ Al at $h=6$ a.u. above the B site on a plane 3 a.u. above the surface. (c) Total charge density in a vertical plane for the graphite $+(2\times2)$ Al system at $h=6$ a.u. above the H site. Solid and dotted contours correspond to positive and negative values of the difference, respectively. The contour spacings are, respectively, 2×10^{-3}, 2×10^{-3}, and 8×10^{-3} electrons/(a.u.)^3. Small arrows point towards increasing density.

This leads to net binding, i.e., negative $\Delta E(h)$. The charge accumulation between the tip and sample surface occurs even for a larger value of h, as shown in Fig. 5(b). These results are qualitatively similar to those obtained earlier for a (1×1) array of carbon tip atoms.[20] Note that a bond localized between the tip and sample requires the admixture of states from both sides. In what follows we examine localized states contributing to such bonds.

In order to reveal the origin of states, which form as a result of the tip-sample interaction, we present the band structure of the graphite monolayer folded into BZ corresponding to the (2×2) supercell in Fig. 6. The scheme of folding from the actual surface BZ of graphite to that of the (2×2) supercell is also shown in the same figure. The states (π and π^*) crossing the Fermi level at the usual K point of graphite are folded to $\bar{K}$, but states at the M point are folded to the $\bar{\Gamma}$ point of the supercell BZ. The band structure shown in Fig. 6 is in good agreement with previous calculations.[5,15,46] Besides the well-known σ, π, and π^* states, it reproduces the surface states (labeled by S) first identified in Ref. 46. In Figs. 7 and 8 we present the evolution of states near the Fermi level computed for the graphite $+(2\times2)$ Al system at the $\bar{\Gamma}$ and $\bar{K}$ points of the supercell BZ. In accordance with the simple arguments at the beginning of this section, as h decreases the tip and graphite states shift and split apart in energy, and some graphite-derived states which are normally unoccupied dip below the Fermi level. This gives rise to significant changes in $\Delta\rho(\mathbf{r})$. For states lying deep in the valence band interaction effects are weaker in the intermediate range of h. The effect of the tip on states at the

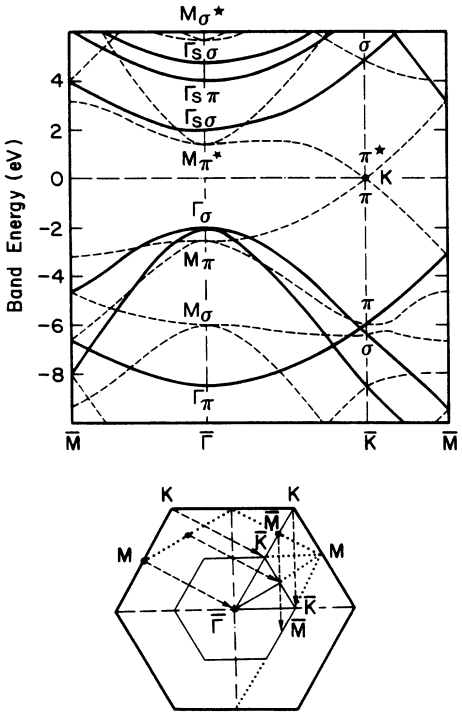

FIG. 6. Energy band structure of the free graphite monolayer folded into the two-dimensional Brillouin zone of the (2×2) supercell. The dashed lines are the folded bands with their nature indicated at the symmetry points. The zero of energy is set at the Fermi level. Bottom: correspondence between the symmetry points of the (1×1) and (2×2) Brillouin zones.

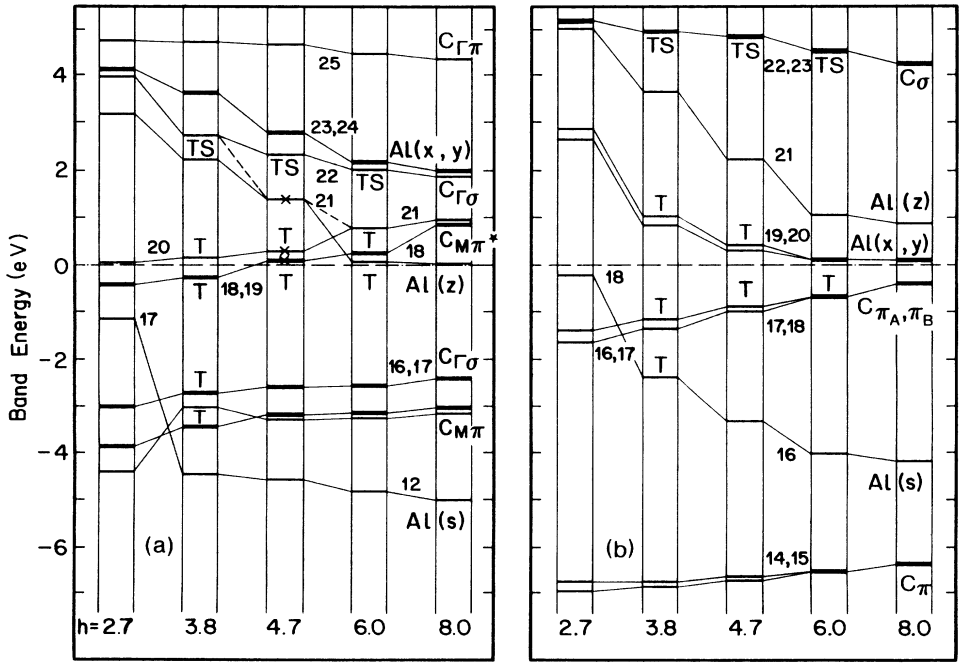

FIG. 7. The evolution of the zone folded states of the graphite $+(2\times2)$ Al system as a function of h for Al above the B site, obtained from SCF pseudopotential calculations at (a) $\bar{\Gamma}$; (b) $\bar{K}$. States which are degenerate or very close in energy are shown by thick bars; numerals denote band indices. Tip-induced localized states TILS are marked by T, whereas surface states modified by the tip are marked by TS. C_M denotes the graphite states originating from the M point of the (1×1) BZ. Crosses indicate states whose charge distributions are plotted in Fig. 9.

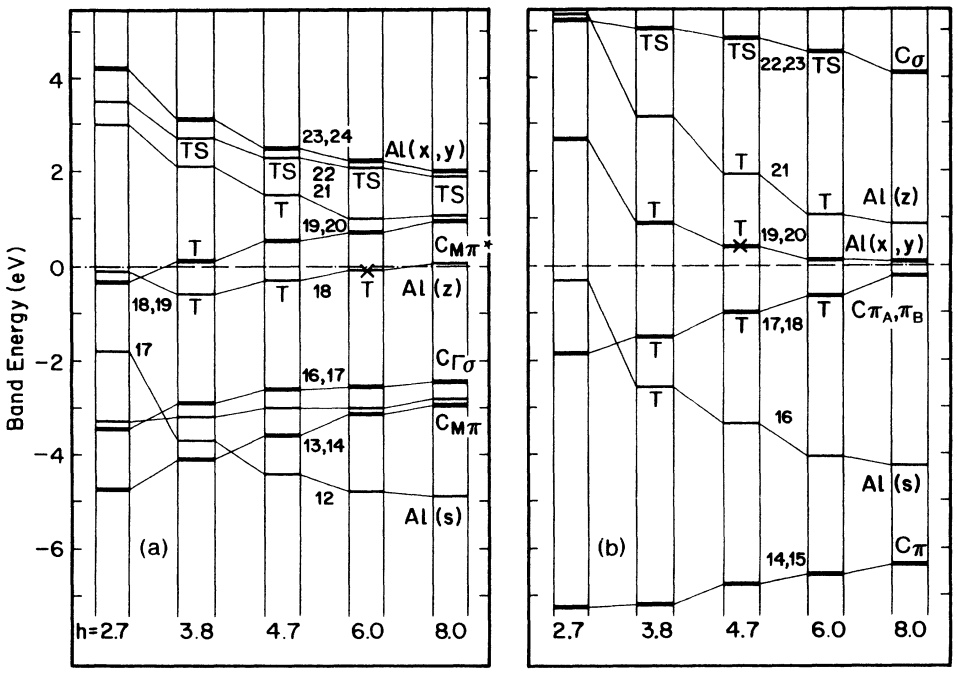

FIG. 8. Same as Fig. 7, except that the Al atom is above the H site.

$\bar{K}$ point is essentially the same at the B and H sites, except for the small splitting of the otherwise degenerate π and π^* states at the K point for the B site. Interestingly, tip-surface interaction effects are more complicated at the $\bar{\Gamma}$ point. In particular Al $p_{x,y}$ states mix strongly with M-derived π^* states of graphite above the Fermi level. The interaction is so strong that for $h<6$ a.u. two unoccupied M-derived π^* states form a bonding combination by acquiring an appreciable admixture of Al $p_{x,y}$ orbitals and dip below the Fermi level. Below the minimum of $\Delta E(h)$ ($h \lesssim 4$ a.u.) the evolution of the states is no longer continuous and involves states further away from the Fermi level. Thus Al-s states interact with the graphite s-like states, and the antibinding combination constructed therefrom rises towards E_F and crosses several graphite states. However, in this range of h the tip-sample system is expected to undergo strong deformations to accommodate huge interatomic forces and to lower the total energy, leading to further rearrangement of the states.

The tip and sample states near the Fermi level already exhibit a good deal of mixing in the range $4<h<6$ a.u. These states, which are identified as the tip-induced localized states, should play a crucial role in STM. Electrostatic splitting between graphite $K\pi$ and Al p states near E_F and changes in the graphite surface states above the potential barrier between the tip array and the sample surface are noticeable even for $h=8$ a.u. Because of this mixing and also the spurious interactions in the tip array, the Al p_z and $p_{x,y}$ states, which are normally degenerate in the free Al atom, exhibit a significant splitting at large h. Since these states have a small dispersion compared to the graphite bands near E_F, and thus a higher density of states, the Fermi level for $h \geq 6$ a.u. is pinned at the $\bar{K}$ point between the lowest Al and the graphite π^* states, but closer to the former. On the other hand, for $h<6$ a.u. states derived from a combination of the above cross the Fermi level not only at the B site, but also at the H site. However, in view of the fact that the tip in a real STM experiment is only a local perturbation on the macroscopic sample surface, the common Fermi level of a real graphite sample and Al tip under an infinitesimal bias has to coincide with E_F of the free graphite. Nevertheless, electrostatic energy splittings due to local charge transfer between tip and sample made of different materials are expected. For graphite, where the degenerate π states at the K point with nodes at particular top sites play a dominant role,[12,15,16,21] their shift below E_F will produce an asymmetric I-V characteristic. Because the $M\pi^*$-derived states have a different nodal structure they can even alter the qualitative appearance of STM images.

In Fig. 9 the charge distributions of TILS with varying orbital character, which are formed from the bonding and antibonding combination of graphite and Al states, exhibit characteristic patterns. The important feature common to all these states is that more charge is located on the graphite side than about the Al tip atom. This is an expected trend because carbon is more electronegative than Al. In terms of the simple two-level analysis presented above, $\varepsilon_t > \varepsilon_s$ implies charge transfer towards the graphite. We also compared selected states with those obtained with the multiatom tip [i.e., graphite $+(3\times3)$ Al_4 model] and could conclude that the outermost tip atom predominantly interacts with the sample, since the character of most TILS was maintained with the multiatom tip. The antibonding nature of the state in Fig. 9(a), which derives from a combination of M-derived

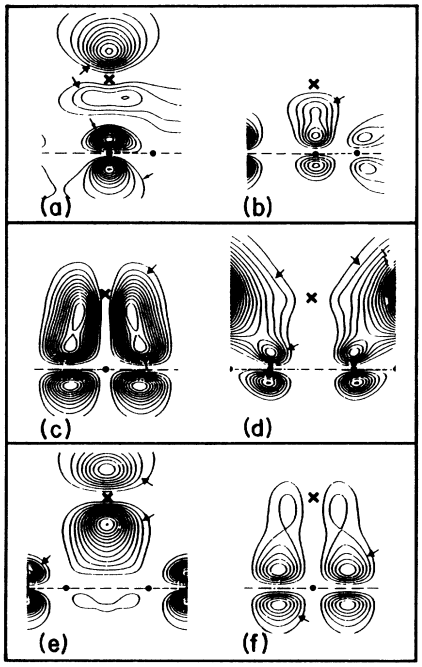

FIG. 9. Charge-density contours of typical tip-induced localized states (TILS) with energies near E_F for the graphite $+(2\times2)$ Al system. (a) $\bar{\Gamma}$-21 yz, B site, $h=4.7$ a.u., contour spacing $\delta\rho=2\times10^{-3}$ electrons/(a.u.)^3. (b) $\bar{\Gamma}=20$ yz, B site, $h=4.7$ a.u., $\delta\rho=2\times10^{-3}$. (c) $\bar{\Gamma}$-18 xz, B site, $h=4.7$ a.u., $\delta\rho=5\times10^{-4}$. (d) $\bar{K}$-19 yz, H site, $h=4.7$ a.u., $\delta\rho=10^{-4}$. (e) $\bar{\Gamma}$-18 yz, H site, $h=6$ a.u., $\delta\rho=10^{-4}$. (f) $\bar{\Gamma}$-19 xz, B site, $h=6$ a.u., $\delta\rho=10^{-3}$.

graphite and Al p_z states, is clear from the reduced charge at the center of the carbon—Al bond. By contrast, the analogous state in Fig. 9(b) displays a bonding character with a significant charge transferred to the graphite site. Following the evolution of states in Fig. 7(a), we also see that the state shown in Fig. 9(c) displays a bonding character between the graphite $M\pi^*$ and the Al p_x orbitals. The state at the K point of the H site in Fig. 9(d) is a bonding combination of one graphite $K\pi$ and of the Al p_y state. That tip-induced localized states can occur even at $h=6$ a.u. is demonstrated in Fig. 9(e). This bonding combination of still another graphite $M\pi^*$ and of the Al p_z states, which is just below E_F, contributes a significant amount of charge above the center of the surface hexagon. Note that this site normally has vanishingly small charge density in the free graphite surface. The contour plots in Figs. 9(c), 9(d), and 9(f) give an idea of a striking effect that TILS should have in STM. Such x,y-like states should have significant tunneling matrix elements,[4] although they do not contribute to the local density of states at the center of the tip, i.e., the tunneling current within the Tersoff-Hamann theory,[3] even if it is generalized to include z-like ($m=0$) states. Finally the state shown in Fig. 9(f), which has the same character as the state in Fig. 9(c), shows an appreciable Al p_x admixture even for the tip 6 a.u. above the surface at the B site.

In view of the above discussion, it becomes clear that the situation for the interacting tip-sample system is quite different from that commonly assumed, where the tip and sample states near E_F are weakly overlapping on a dividing surface passing through the potential barrier.[3–6] Figure 4 shows that as h decreases a classically allowed channel forms and the tip-sample interaction gradually increases. Owing to the strong local tip-sample interaction the parallel-momentum vector $\mathbf{k}_\parallel$, which is normally conserved in the independent electrode regime, is no longer a good quantum number. Already, in the intermediate range of h ($4\lesssim h\lesssim 6$) the difference between $\Phi_a=\Phi+k_\parallel^2$ and the potential barrier Φ is substantially reduced, and the tip and the sample are electronically connected by TILS. On the other hand, the energy of the lowest propagating state in the channel increases owing to its lateral confinement. Even if the potential in the channel is lower than E_F, the states of electrodes near E_F may encounter a finite barrier[25,29,46] denoted as the effective barrier Φ_{eff}. The difference $\Phi_{\text{eff}}-\Phi$ is positive and site-dependent but diminishes as $h\to\infty$. This implies that prior to the initiation of a point contact the current is still tunneling even if the local potential barrier Φ already collapses in the range of increasing attractive force. The formation of TILS imposes local modifications in the local density and character of states near E_F, which determines the tunneling current. Because of a small but finite tunneling barrier between the electrodes the transmission is also affected. Moreover, these modifications are site specific and thus vary depending on the position of the tip. Therefore, perturbation theories of STM (Refs. 3, 5, 15, and 16) must be modified, in particular, the corrugation obtained in STM measurements can markedly deviate from that of $\rho(\mathbf{r}_0,E_F)$ at small h. Even though the tunneling from the base of the outermost tip atom can be treated within a perturbation scheme, the inclusion of TILS even in the tunneling range is not straightforward for the following reasons. First, the character of TILS varies depending upon the location of the tip and the energy and momentum of the parent sample states. This requires a detailed account of relevant electronic states over the BZ. Secondly, the transfer Hamiltonian approach,[11] which is based on the assumption that tip and sample states weakly overlap on a dividing plane, may not be adequate for small enough h. In other words, the tunneling current has to be calculated by going beyond first-order perturbation theory. In principle, the tunneling current can be calculated by evaluating the current operator for a combined tip-sample system.[6] However, such a calculation is not feasible if tip-sample interaction effects on the atomic scale are included as in the present study. In a recent study,[21] to judge qualitative trends and to reveal the relevant contribution of TILS, the effect of the tip was first included as a local perturbation on the sample. Then, in addition to unperturbed sample and tip states, TILS were included in the transfer Hamiltonian approach. In the expression for the tunneling current derived within first-order time-dependent perturbation theory the effect of TILS is included in terms of their overlap integral with the free sample states $\langle\varphi_s|\varphi_{\text{TILS}}\rangle$. Using an empirical tight-binding method it was shown that in the presence of TILS the tunneling current can be strongly enhanced and

the corrugation deduced from $\rho_s(\mathbf{r}_0, E_F)$ is significantly underestimated.[21]

The effective barrier Φ_{eff} diminishes as the potential in the dividing plane $V(x,y,z=h/2)$ approaches those of the electrodes if h is further decreased until a well-defined bond forms. This way an electronic orifice between the tip and the sample surface is formed and hence a point contact is initiated leading to quantum ballistic transport.[47] In this range of h ($h \lesssim 4$ a.u.) the character of the conductance should undergo a drastic change,[47–51] as in experiments on metals,[24] but its behavior will also depend on the plastic deformation induced by the tip.[24,30,51]

V. CONCLUSIONS

In this paper we have investigated various tip-sample interaction effects by performing *ab initio* force and electronic structure calculations on graphite-sample and aluminum-tip model systems. Important conclusions are drawn from this study. (i) In spite of the fact that the graphite surface is rather inert, its interaction with an Al atom is significant and results in a bond with a binding energy of 0.33 eV at the top site and 0.61 eV at the hollow site. (ii) The ion-ion repulsion plays a dominant role in determining the corrugation in all AFM modes in the repulsive and strongly attractive ranges. The reversed corrugation, i.e., minimum attraction at the top rather than hollow site predicted beyond maximum attraction could be detected with a stiff cantilever as in Ref. 26. (iii) Attraction by tip atoms far from the outermost one can make important contributions to the total tip force. In some cases, their contribution might become so dramatic that while the total tip force is attractive, the outermost tip atom is in the strong repulsive-force region causing plastic deformation of the sample surface. Therefore the repulsive force on the outermost tip atom is always underestimated in AFM measurements. Nevertheless variations of the force on the tip as it is scanned along the sample and its perpendicular gradient, i.e., the quantities recorded in AFM are dominated by short-range forces which are adequately predicted by calculations such as ours. Present results suggest that a sharp tip with a single atom at its apex is able to yield atomic resolution in a truly nondestructive mode provided that the tip-surface distance is chosen appropriately. The images and the resolution that are obtained with flat tips having several atoms at its apex, however, are distorted and complicated, and require a detailed Fourier analysis.[33] (iv) The most fundamental effects of tip-sample interaction are found in the electronic structure even for an inert sample surface like graphite. Owing to the close proximity of the tunneling tip, tip and sample states are strongly perturbed and hence are combined to form new states localized near the tip whose energies, charge distributions, and amplitudes depend on the position of the latter along and perpendicular to the sample. As a result the local density of states are modified and new tunneling matrix elements, e.g., between x,y-like states become important. Graphite states at the M point of the BZ which have high density ~ 1 eV above the Fermi level become, in particular, involved in the formation of localized states. Therefore one expects that at small tip-sample separations STM images will deviate in a characteristic but complicated way from those predicted for well-separated electrodes,[5,12,15] even prior to repulsive contact. Judging from combined STM-AFM measurements,[18] and in view of the particularly low unperturbed density of states of pristine graphite at E_F, such effects are likely to distort images recorded under typical STM operating conditions (1 nA, 10–100 mV).[7–10,13–15] Obviously, this deserves more attention.

ACKNOWLEDGMENTS

The authors thank H. Rohrer and T. Schneider for their interest in this work in addition to J. Behm and U. Dürig for discussing results prior to publication. One of us (S.C.) gratefully acknowledges the financial support and hospitality of the IBM Zurich Research Laboratory, and wishes to thank E. P. Stoll for his valuable assistance.

*Permanent address: Department of Physics, Bilkent University, Bilkent, 06533 Ankara, Turkey.

[1] G. Binnig, H. Rohrer, Ch. Gerber, and E. Weibel, Phys. Rev. Lett. **49**, 57 (1982); G. Binnig and H. Rohrer, IBM J. Res. Dev. **30**, 1 (1986); G. Binnig and H. Rohrer, Rev. Mod. Phys. **59**, 615 (1987).

[2] G. Binnig, C. F. Quate, and Ch. Gerber, Phys. Rev. Lett. **56**, 930 (1986).

[3] J. Tersoff and D. R. Hamann, Phys. Rev. Lett. **50**, 1998 (1983); Phys. Rev. B **31**, 805 (1985).

[4] A. Baratoff, Physica B+C **127B**, 143 (1984).

[5] A. Selloni, P. Carnevali, E. Tosatii, and C. D. Chen, Phys. Rev. B **31**, 2602 (1984); see, however, **34**, 7406 (1986).

[6] N. D. Lang, Phys. Rev. Lett. **56**, 1164 (1986); Phys. Rev. B **34**, 5947 (1986); Phys. Rev. Lett. **58**, 45 (1987).

[7] Proceedings of the IBM Europe Institute on Scanning Tunneling Microscopy [IBM J. Res. Dev. **30**, 353 (1986)].

[8] Proceedings of the 1st International Conference on Scanning Tunneling Microscopy [Surf. Sci. **181**, 1 (1987)].

[9] Proceedings of the 2nd International Conference on Scanning Tunneling Microscopy [J. Vac. Sci. Technol. A **6**, 257 (1988)].

[10] Proceedings of the 3rd International Conference on Scanning Tunneling Microscopy [J. Microscopy **152**, 1 (1988)].

[11] J. Bardeen, Phys. Rev. Lett. **6**, 57 (1961).

[12] J. Tersoff, Phys. Rev. Lett. **57**, 440 (1986).

[13] G. Binnig, H. Fuchs, Ch. Gerber, H. Rohrer, E. Stoll, and E. Tosatti, Europhys. Lett. **1**, 31 (1985).

[14] I. P. Batra, N. Garcia, N. Rohrer, H. Salemink, E. Stoll, and S. Ciraci, Surf. Sci. **181**, 126 (1987).

[15] D. Tomanek, S. G. Louie, H. J. Mamin, D. W. Abraham, R. E. Thompson, E. Ganz, and J. Clarke, Phys. Rev. B **35**, 7790 (1987); D. Tomanek and S. G. Louie, *ibid.* **37**, 8327 (1988); see also R. C. Tatar and S. Rabii, *ibid.* **25**, 4126 (1982).

[16] H. Mizes, Sang-Il Park, and W. Harrison, Phys. Rev. B **36**, 4491 (1987).

[17] J. M. Soler, A. M. Baro, N. Garcia, and H. Rohrer, Phys. Rev. Lett. **57**, 444 (1986).

[18] U. Dürig, J. K. Gimzewski, and D. W. Pohl, Phys. Rev. Lett.

57, 2403 (1986); H. Yamada, T. Fujii, and K. Nakayama, J. Vac. Sci. Technol. A **6**, 293 (1988).

[19]G. Binnig, Ch. Gerber, E. Stoll, T. R. Albrecht, and C. F. Quate, Europhys. Lett. **3**, 1281 (1987); T. R. Albrecht and C. F. Quate, J. Vac. Sci. Technol. A **6**, 271 (1988); R. Erlandsson, G. M. McClelland, C. M. Mate, and S. Chiang, *ibid.* **6**, 266 (1988); H. Herzelmann, E. Meier, P. Grütter, H.-R. Hidber, L. Rosenthaler, and H.-J. Güntherodt, J. Vac. Sci. Technol. A **6**, 275 (1988); O. Marti, B. Drake, S. Gould, and P. K. Hansma, *ibid.* **6**, 287 (1988).

[20]S. Ciraci and I. P. Batra, Phys. Rev. B **36**, 6194 (1987); I. P. Batra and S. Ciraci, J. Vac. Sci. Technol. A **6**, 313 (1988).

[21]E. Tekman and S. Ciraci, Phys. Scr. **38**, 486 (1988); E. Tekman, M. Sc. thesis, Bilkent University, 1987; E. Tekman and S. Ciraci, Phys. Rev. B **40**, 10 286 (1989).

[22]H. A. Mizes and W. A. Harrison, J. Vac. Sci. Technol. A **6**, 300 (1988).

[23]G. Binnig, N. Garcia, H. Rohrer, J. M. Soler, and F. Flores, Phys. Rev. B **30**, 4816 (1984).

[24]J. K. Gimzewski and R. Möller, Phys. Rev. B **36**, 1284 (1987).

[25]N. D. Lang, Phys. Rev. B **36**, 8173 (1987); **37**, 10 395 (1988).

[26]U. Dürig, O. Züger, and D. W. Pohl, J. Microscopy **152**, 259 (1988).

[27]V. M. Hallmark, S. Chiang, J. F. Rabolt, J. D. Swalen, and R. J. Wilson, Phys. Rev. Lett. **59**, 2879 (1987).

[28]J. Wintterlin, J. Wiechers, H. Brune, T. Gritsch, H. Höfer, and R. J. Behm, Phys. Rev. Lett. **62**, 59 (1989).

[29]S. Ciraci, A. Baratoff, and I. P. Batra, Bull. Am. Phys. Soc. **34**, 538 (1989); (unpublished).

[30]J. P. Pethica, Phys. Rev. Lett. **57**, 3235 (1986); for the related instability, see J. B. Pethica and W. C. Oliver, Phys. Scr. **19A**, 61 (1987).

[31]H. J. Mamin, E. Ganz, D. W. Abraham, R. E. Thomson, and J. Clarke, Phys. Rev. B **34**, 9015 (1986).

[32]F. Abraham, I. P. Batra, and S. Ciraci, Phys. Rev. Lett. **60**, 1314 (1988).

[33]F. Abraham and I. P. Batra, Surf. Sci. **209**, L125 (1989).

[34]A. Baratoff, G. Benedek, and I. P. Batra, Europhysics Conf. Abstracts **121**, 64 (1988). The quoted force values should be divided by $\simeq 5$.

[35]A. Bryant, D. P. E. Smith, and C. F. Quate, Appl. Phys. Lett. **48**, 832 (1986).

[36]Sang-Il Park and C. F. Quate, Appl. Phys. Lett. **48**, 112 (1986); R. Sonnenfeld and P. K. Hansma, Science **232**, 211 (1986).

[37]M. Schlüter, J. R. Chelikowsky, S. G. Louie, and M. L. Cohen, Phys. Rev. B **12**, 4200 (1975).

[38]D. R. Hamann, M. Schlüter, and C. Chiang, Phys. Rev. Lett. **43**, 1494 (1979).

[39]J. Ihm, A. Zunger, and M. L. Cohen, J. Phys. C **12**, 4409 (1979); M. T. Yin and M. L. Cohen, Phys. Rev. B **26**, 3259 (1982).

[40]I. P. Batra, S. Ciraci, G. P. Srivastava, J. S. Nelson, and C. Y. Fong, Phys. Rev. B **34**, 8246 (1986).

[41]M. T. Yin and M. L. Cohen, Phys. Rev. B **29**, 6996 (1984).

[42]I. P. Batra and S. Ciraci, Phys. Rev. B **33**, 4312 (1986).

[43]E. Zaremba and W. Kohn, Phys. Rev. B **15**, 1769 (1977).

[44]J. Harris and A. Liebsch, J. Phys. C **15**, 2275 (1982).

[45]H. Hellmann, *Einführung in die Quantentheorie* (Deuticke, Leipzig, 1937); R. P. Feynman, Phys. Rev. **56**, 340 (1939); J. C. Slater, J. Chem. Phys. **57**, 2389 (1972).

[46]M. Posternak, A. Baldereshi, A. J. Freeman, and E. Wimmer, Phys. Rev. Lett. **52**, 863 (1984).

[47]Yu. V. Sharvin, JETP Lett. **21**, 655 (1965); L. I. Glazman, Lesovik, D. E. Khmelnitskii, and R. I. Shekhter, Sov. Phys.—JETP **48**, 238 (1989).

[48]N. Garcia (unpublished).

[49]E. Tekman and S. Ciraci, Phys. Rev. B **39**, 8772 (1989); **40**, 8559 (1989).

[50]S. Ciraci, in Basic Concepts and Applications of Scanning Tunneling Microscopy and Related Techniques, edited by H. Rohrer, N. Garcia, and J. Behm (Kluwer Academic, Amsterdam, in press).

[51]S. Ciraci and E. Tekman, Phys. Rev. B **40**, 11 969 (1989).